INTERNATIONAL JOURNAL FOR NUMERICAL METHODS IN FLUIDS
Int. J. Numer. Meth. Fluids 2010; **63**:431–448
Published online 2 June 2009 in Wiley InterScience (www.interscience.wiley.com). DOI: 10.1002/fld.2086

Beating capillarity in thin film flows

Mathieu Sellier[1,*,†] and Satyananda Panda[2]

[1]*Department of Mechanical Engineering, University of Canterbury, Private Bag 4800, Christchurch 8140, New Zealand*
[2]*Department of Mathematics, National Institute of Technology, Calicut NIT Post. 673601, Kerala, India*

SUMMARY

The combination of substrate unevenness and capillarity is known to induce far-reaching perturbations at the free surface of thin liquid films. These might be undesired and this paper explores the possibility to control the free surface of thin liquid films to give it a prescribed profile by a suitable design of the underlying substrate. This corresponds to the inverse of the widely studied forward problem, which considers the effect of substrate unevenness on a free surface. Assuming that the steady free surface profile can be described by the lubrication approximation, this optimal control problem is shown to be governed by a first-order partial differential equation, which is solved numerically using the method of characteristics. The proposed method is successfully tested for a range of desired free surface profiles and the domain of existence of a solution to the inverse problem is probed. Expectedly, it is shown that, owing to surface tension, not all free surface profiles can be achieved but in some cases capillarity can be beaten and a prescribed free surface profile obtained. Copyright © 2009 John Wiley & Sons, Ltd.

Received 7 December 2008; Revised 5 April 2009; Accepted 9 April 2009

KEY WORDS: thin film flows; inverse problems; flow control; surface reconstruction; capillarity

1. INTRODUCTION

It is common knowledge that the interface between two fluids cannot form sharp corners. This is a consequence of interfacial tension (or capillarity) tending to smooth corners to reduce the curvature of the interface. A natural question one might ask is whether capillarity can be beaten and sharp corners made to appear. More generally, one might wonder whether it is possible to control the interface between two fluids. This problem is investigated here in the context of thin liquid films where one of the fluid is a liquids flowing over a solid substrate and the other is a passive gas. In that case, the interface is actually a free surface. Beyond the mere interest of the scientific question, several applications relevant to coating processes, in particular, rely on the ability to control the

*Correspondence to: Mathieu Sellier, Department of Mechanical Engineering, University of Canterbury, Private Bag 4800, Christchurch 8140, New Zealand.
†E-mail: mathieu.sellier@canterbury.ac.nz

fluid–fluid interface. The final appearance of a layer coated for decorative purposes, for example, depends directly on the shape of the free surface. Another motivation comes from the rising number of thin film devices that are manufactured in industries as diverse as microelectronics, displays, optical storage, or microfluidic devices. All these require an understanding and a control of the thin layer deposition process and of the free surface profile, [1].

Various approaches have been proposed in the past to control the free surface of liquid films. Typically, flow control can be achieved by the application of a body force or an appropriate perturbation of the domain boundary. Examples of the former include active control of the free surface disturbance by means of Marangoni stresses induced by localized heaters, [2], or increasing the normal component of gravity, [3]. The results reported recently by Tseluiko *et al.* in [4] show that the application of an electric field can also suppress free surface defects induced by step topographies. All these have, however, limited applicability when it comes to the precise control of the free surface profile over a wide range. The approach adopted here belongs to the latter class of flow control as it consists in seeking substrate profiles capable of deforming the free surface in a desired way. Decré and Baret first suggested in [1] that free surface defects generated by topographic features could be removed by an appropriate patterning of the substrate. Preliminary results reported by Gaskell *et al.* in [5], on a trial-and-error basis, confirmed that free surface disturbances caused by a square peak topography could be reduced by modifying the topography surrounding the peak. Recently, it has been shown in [6] that for planar flows, it is possible to precisely control the free surface profile of a thin film by an appropriate design of the substrate. An explicit formula is derived for the required substrate profile. The latter allows the discrimination between achievable and non-achievable free surface profiles. This paper extends to the three-dimensional flows technique proposed in [6] to control the free surface of thin liquid films.

The problem at hand falls into the category of optimal shape design for which one seeks the optimal substrate design to control flow features. Such problems are often analyzed in the framework of PDE-constrained optimization. Classically, an objective function is defined and the governing equations (or state equations) are treated as constraints to the optimization problem, [7, 8]. We show in this paper that the optimal design problem is explicitly governed by a first-order partial differential equation (pde), which can be solved numerically. The method proposed here could be adapted to other inverse problems relevant to thin layer flows such as bedrock reconstruction in glacier flows, or riverbed reconstruction from free surface data.

The next section briefly describes the forward problem, which consists in finding the free surface profile for a given substrate topography. The notations and governing equations are introduced, the solution strategy, and sample results reported. The main contribution of the paper is in the following section where the approach to solve the inverse problem, which consists in finding the substrate topography inducing the desired free surface profile is described. The penultimate section gives validating results and probes the existence space of the solution to the inverse problem. Finally, conclusions are drawn.

2. THE FORWARD PROBLEM

The problem at hand is sketched in Figure 1. A thin liquid layer runs down an inclined plane over an uneven substrate. The shape of the free surface results from the competition between the substrate features tending to impress their shapes on the free surface and the surface tension

DOI: 10.1002/fld

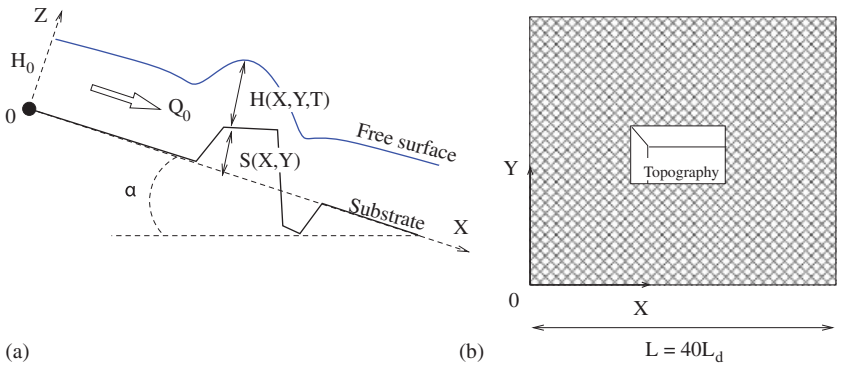

Figure 1. Schematic diagram of the problem considered and the corresponding notations: (a) side view and (b) top view.

tending to flatten it. Capillary waves develop as a result of this interaction and cause far-reaching free surface disturbances, which may be highly undesirable.

2.1. The governing equations

The flow of a thin liquid film draining down a plane inclined at an angle α to the horizontal with a constant flux Q_0 is described in the present work by the lubrication approximation. The fluid has viscosity μ, density ρ, and surface tension σ. This approximation which has been used extensively to analyze a range of thin film flow problems provides a pair of non-linear evolution equations for the film thickness $H(X, Y, T)$ and the pressure $P(X, Y, T)$, which is constant across the thickness to leading order. The coordinates (X, Y) are in the substrate plane, X being in the flow direction as shown in Figure 1. Although the flows considered here are steady and therefore do not depend on the time T, the steady solution is obtained by solving the transient equations for a long enough time to reach a steady state.

The first of these equations expresses the conservation of mass and reads as

$$\frac{\partial H}{\partial T} = -\nabla \cdot \mathbf{Q} \tag{1}$$

$$\mathbf{Q} = -\left(\frac{H^3}{3\mu}(\nabla P - \rho g \sin(\alpha)\mathbf{i})\right) \tag{2}$$

where $\mathbf{Q} = (Q_x, Q_y)$ is the discharge and g the standard gravity ($9.81\,\mathrm{m/s^2}$). The second equation expresses the balance of normal stresses at the interface. Accordingly,

$$P + \sigma\nabla^2(H + S) - \rho g \cos(\alpha)(H + S) = 0 \tag{3}$$

$S(X, Y)$ is the topography function, which describes the substrate topography as illustrated in Figure 1. The second term on the left-hand side of Equation (3) is the linearized capillary pressure and the third is that due to gravity acting in the direction normal to the flow.

DOI: 10.1002/fld

Scaling the film thickness with that of the fully developed flow $H_0=(3\mu Q_0/\rho g\sin(\alpha))^{1/3}$, the coordinates (X,Y) with the dynamic capillary length $L_d=(\sigma H_0/3\rho g\sin(\alpha))^{1/3}$, and the time with $T_0=L_d/U_0$ where $U_0=3Q_0/2H_0$, the dimensionless counterpart of Equations (1)–(3) are:

$$\frac{\partial h}{\partial t}=-\nabla\cdot\mathbf{q} \tag{4}$$

$$\mathbf{q}=-\left(\frac{h^3}{3}(\nabla p-2\mathbf{i})\right) \tag{5}$$

$$p=-6\nabla^2(h+s)+2\sqrt[3]{6}Ca^{1/3}\cot(\alpha)(h+s) \tag{6}$$

The dimensionless term $Ca=\mu U_0/\sigma$ is known as the Capillary number and expresses the ratio of viscous to surface tension stresses. A detailed asymptotic analysis reveals that the lubrication approximation holds for low value of the Capillary number ($Ca\ll 1$) and small values of $\varepsilon^2 Re$, where Re is the Reynolds number and $\varepsilon=H_0/L_0$ is a small number compared with one. The flow is assumed fully developed upstream such that $h(x=0,y,t)=1$ and $\nabla p\cdot\mathbf{n}=0$, where $\mathbf{n}$ is the normal to the boundary pointing outward. All other boundaries assume natural boundary conditions, i.e. $\nabla h\cdot\mathbf{n}=\nabla p\cdot\mathbf{n}=0$.

2.2. Solution method

The forward problem consists in finding the film thickness for a given substrate profile. It has recently been extensively studied experimentally, [1, 9, 10], theoretically, [11–13], or numerically [3, 5, 14–18]. The finite element package COMSOL is used here to solve the governing equations on the solution domain. The ability of this commercial package to accurately solve the pertaining governing equations has recently been demonstrated in [19]. The solution domain is a $40\,L_d\times 40\,L_d$ square. To give a more quantitative idea, this corresponds to a 3.1 cm × 3.1 cm square for a 100 μm thick water film flowing than a plane inclined at 30° to the horizontal.

The governing equations are found easier to implement in COMSOL by introducing the free surface elevation function $\psi(x,y,t)=h(x,y,t)+s(x,y)$ and transforming them in their weak form. The latter is obtained in a standard way by multiplying Equations (4) and (6) by the test functions $u(x,y)$ and $v(x,y)$, respectively, integrating them over the solution domain Ω, and applying Green's first identity to give

$$\int_\Omega\left[u\frac{\partial\psi}{\partial t}-\nabla u\cdot\mathbf{q}\right]\mathrm{d}\omega+\int_\Gamma[u\mathbf{q}\cdot\mathbf{n}]\,\mathrm{d}\gamma=0 \tag{7}$$

$$\int_\Omega[vp-6\nabla v\cdot\nabla\psi-2\times 6^{1/3}Ca^{1/3}\cot(\alpha)v\psi]\,\mathrm{d}\omega+\int_\Gamma[6v\nabla\psi\cdot\mathbf{n}]\,\mathrm{d}\gamma=0 \tag{8}$$

where Γ is the boundary of the computational domain. Incorporating the corresponding boundary conditions, Equations (7) and (8) reduce to

$$\int_\Omega\left[u\frac{\partial\psi}{\partial t}-\nabla u\cdot\mathbf{q}\right]\mathrm{d}\omega+\int_{\Gamma_{\mathrm{out}}}u\frac{2(\psi-s)^3}{3}\,\mathrm{d}\gamma=0 \tag{9}$$

$$\int_\Omega[vp-6\nabla v\cdot\nabla\psi-2\times 6^{1/3}Ca^{1/3}\cot(\alpha)v\psi]\,\mathrm{d}\omega-\int_{\Gamma_{\mathrm{in}}}\left[6v\frac{\partial\psi}{\partial x}\right]\mathrm{d}\gamma=0 \tag{10}$$

DOI: 10.1002/fld

where Γ_{in} is the inflow boundary ($x=0$) and Γ_{out} the outflow boundary ($x=40$). The corresponding weak form of the problem is therefore to find $\psi(x, y, t)$ and $p(x, y, t)$ such that Equations (9) and (10) hold for all time and all possible test functions u and v satisfying the Dirichlet boundary condition. The approximate free surface elevation $\tilde{\psi}$ and pressure $\tilde{p}$ are expressed in terms of the basis functions ϕ_i as follows:

$$\tilde{\psi}(x, y, t) = \sum_{i=1}^{N} \Psi_i(t)\phi_i(x, y) \tag{11}$$

$$\tilde{p}(x, y, t) = \sum_{i=1}^{N} P_i(t)\phi_i(x, y) \tag{12}$$

where N is the number of nodes. Second-order Lagrange basis functions are used leading to a piecewise quadratic description of the free surface elevation and pressure. In the Galerkin formulation used by COMSOL, the test function is chosen to be the basis function. This yields a system of ordinary differential equations for the transient nodal values $\Psi_i(t)$ and $P_i(t)$. COMSOL solves the time-dependent problem using the method of lines. The associated differential algebraic system is solved using DASPK, which employs variable-order, variable-stepsize backward differentiation formulas (BDF). The implicit time-integration generates a non-linear system of equations, which is solved using a Newton iteration and a linear system solver. The default solver parameters (UMFPACK linear solver and a maximum BDF order of 5) were chosen as they appeared to be optimum.

2.3. Sample results

A complete description of the effect of the substrate topography on the free surface can be found in the references cited above. For illustrative purposes and to highlight the motivation for this work, an illustrative result for a square trench topography is presented. The substrate topography is expressed in terms of hyperbolic tangent functions as follows:

$$s_{\tanh}(x, y) = s_0 \left(0.5\left(1+\tanh\left(\frac{x-x_1}{\delta}\right)\right) - 0.5\left(1+\tanh\left(\frac{x-x_2}{\delta}\right)\right)\right) \times \left(0.5\left(1+\tanh\left(\frac{y-y_1}{\delta}\right)\right) - 0.5\left(1+\tanh\left(\frac{y-y_2}{\delta}\right)\right)\right) \tag{13}$$

The parameter s_0 controls the height of the topography, x_1, x_2, y_1, y_2 its location, and δ its steepness. The topography profile can be seen in Figure 2(a) and the parameters are reported in the figure caption. The topography depth is 50% of the film thickness and it extends over 4 L_d. The effect of gravity is ignored and therefore the second term on the right-hand side of Equation (6) is neglected. The corresponding free surface profile can be seen in Figure 2(b). This figure clearly illustrates the far-reaching effect of the topography on the free surface. There is a clear stationary wave upstream of the topography with a bow shape and a bulge of the free surface downstream of the topography. These free surface features are capillary induced. This is the way the free surface has to respond to sustain a rapid height change whilst keeping its curvature as low as possible. The free surface disturbances extend far downstream and may be undesired. This naturally begs the question as to whether it is possible to eliminate them and more generally to control the profile of the free surface.

DOI: 10.1002/fld

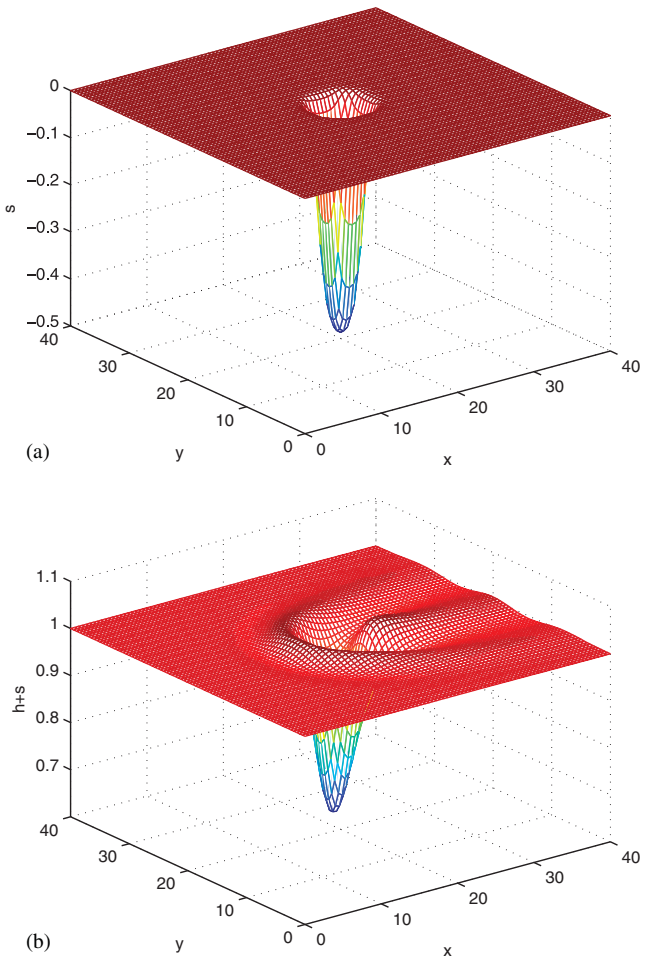

Figure 2. Flow past a square trench. The flow is in the positive x direction: (a) substrate topography according to Equation (13) with $s_0=-0.5$, $x_1=18$, $x_2=22$, $y_1=18$, $y_2=22$, and $\delta=0.8$ and (b) corresponding free surface profile.

3. THE INVERSE PROBLEM

The inverse problem consists in finding the substrate topography $s(x,y)$, which yields the desired free surface profile $w(x,y)$. It is best solved in terms of the free surface elevation function $\psi(x,y,t)$. For the known, desired free surface profile $w(x,y)$, the pressure field is explicitly given by

$$p^{ex}=-6\nabla^2 w+2\sqrt[3]{6}Ca^{1/3}\cot(\alpha)w \tag{14}$$

At steady state, Equations (4) and (5) may be rewritten as

$$\nabla\cdot\left(\frac{(\psi-s)^3}{3}(\nabla p-2\mathbf{i})\right)=0 \tag{15}$$

DOI: 10.1002/fld

Replacing the free surface profile $\psi(x,y)$ by the desired one $w(x,y)$ and applying elementary calculus results in the following pde:

$$\left(\frac{\partial p^{ex}}{\partial x}-2\right)\frac{\partial(\psi-s)}{\partial x}+\left(\frac{\partial p^{ex}}{\partial y}\right)\frac{\partial(\psi-s)}{\partial y}=-\frac{\psi-s}{3}\left(\frac{\partial^2 p^{ex}}{\partial x^2}+\frac{\partial^2 p^{ex}}{\partial y^2}\right) \tag{16}$$

or

$$-\left(\frac{\partial p^{ex}}{\partial x}-2\right)\frac{\partial h}{\partial x}-\left(\frac{\partial p^{ex}}{\partial y}\right)\frac{\partial h}{\partial y}=\frac{h}{3}\left(\frac{\partial^2 p^{ex}}{\partial x^2}+\frac{\partial^2 p^{ex}}{\partial y^2}\right) \tag{17}$$

This is a first-order pde with non-constant coefficients, which involves fourth-order derivatives of the desired free surface profile. It can be solved for $h(x,y)$ using the method of characteristics. Remarkably, while the forward problem involves solving for a non-linear, fourth-order pde, the inverse one only requires the solution to a first order, linear pde. The characteristic curves parameterized by l satisfy the following ordinary differential equations (odes):

$$\frac{\mathrm{d}x}{\mathrm{d}l}=-\left(\frac{\partial p^{ex}}{\partial x}-2\right) \tag{18}$$

$$\frac{\mathrm{d}y}{\mathrm{d}l}=-\frac{\partial p^{ex}}{\partial y} \tag{19}$$

and along the characteristics, the following ode must be fulfilled:

$$\frac{\mathrm{d}h}{\mathrm{d}l}=\frac{h}{3}\left(\frac{\partial^2 p^{ex}}{\partial x^2}+\frac{\partial^2 p^{ex}}{\partial y^2}\right) \tag{20}$$

Interestingly, along the characteristics, we must have

$$\frac{\mathrm{d}x}{-\left(\frac{\partial p^{ex}}{\partial x}-2\right)}=\frac{\mathrm{d}y}{-\frac{\partial p^{ex}}{\partial y}} \tag{21}$$

or equivalently

$$\frac{\mathrm{d}x}{-\frac{h^3}{3}\left(\frac{\partial p^{ex}}{\partial x}-2\right)}=\frac{\mathrm{d}x}{q_x}=\frac{\mathrm{d}y}{-\frac{h^3}{3}\frac{\partial p^{ex}}{\partial y}}=\frac{\mathrm{d}y}{q_y} \tag{22}$$

which shows that the characteristics are nothing but the depth-averaged streamlines of the flow (based on (q_x,q_y)). The fact that these depth-averaged streamlines cannot intersect in the lubrication approximation framework precludes the existence of shocks or rarefaction in the solution.

An other interesting point is observed by rearranging Equation (20) such that

$$\frac{\mathrm{d}h}{h}=\frac{1}{3}\left(\frac{\partial^2 p^{ex}}{\partial x^2}+\frac{\partial^2 p^{ex}}{\partial y^2}\right)\mathrm{d}l \tag{23}$$

DOI: 10.1002/fld

which, using Equations (18) and (19), may be rewritten as follows:

$$\frac{\mathrm{d}h}{h} = -\frac{1}{3}\frac{\dfrac{\partial^2 p^{ex}}{\partial x^2}}{\left(\dfrac{\partial p^{ex}}{\partial x} - 2\right)}\mathrm{d}x - \frac{1}{3}\frac{\dfrac{\partial^2 p^{ex}}{\partial y^2}}{\dfrac{\partial p^{ex}}{\partial y}}\mathrm{d}y \tag{24}$$

or equivalently

$$\mathrm{d}(\ln h) = \frac{\partial\left(-\dfrac{1}{3}\ln\left(\dfrac{\partial p^{ex}}{\partial x} - 2\right)\right)}{\partial x}\mathrm{d}x + \frac{\partial\left(-\dfrac{1}{3}\ln\left(\dfrac{\partial p^{ex}}{\partial y}\right)\right)}{\partial y}\mathrm{d}y \tag{25}$$

We can now distinguish two cases:

- If the cross-flow pressure gradient vanishes ($\partial p^{ex}/\partial y = 0$), the streamlines are in the positive x-direction and $\mathrm{d}y$ is equal to zero in Equation (25) according to Equation (19). Equation (25) reduces to an ode, which can easily be integrated to yield

$$h^3 = \frac{K}{\left(\dfrac{\partial p^{ex}}{\partial x} - 2\right)} \tag{26}$$

  a result identical to the one found in [6] for planar flows where K is an integration constant.
- If the cross-flow pressure gradient is non-zero, integration along a characteristic curve C gives

$$\ln h = -\frac{1}{3}\ln\left(\frac{\partial p^{ex}}{\partial x} - 2\right) + g(y) - \frac{1}{3}\ln\left(\frac{\partial p^{ex}}{\partial y}\right) + f(x) \tag{27}$$

  where $f(x)$ and $g(y)$ are integration functions, which are found by matching the solutions between regions where a cross-flow pressure gradient exists and those where it is does not. Equation (27) can be rewritten as

$$h^3 = \frac{\exp\left(\dfrac{(f(x)+g(y))}{3}\right)}{\dfrac{\partial p^{ex}}{\partial y}\left(\dfrac{\partial p^{ex}}{\partial x} - 2\right)} \tag{28}$$

Since there always exists a unique real cube root, this result proves the existence and uniqueness of a solution. However, nothing precludes the film thickness h from being negative, which would be unrealistic.

Although insightful, the previous analysis does not easily lend itself to a practical solution to the inverse problem. Instead, the system of odes, Equations (18)–(20), is solved numerically using a simple, explicit finite difference scheme. Accordingly, the characteristics and the solutions along

DOI: 10.1002/fld

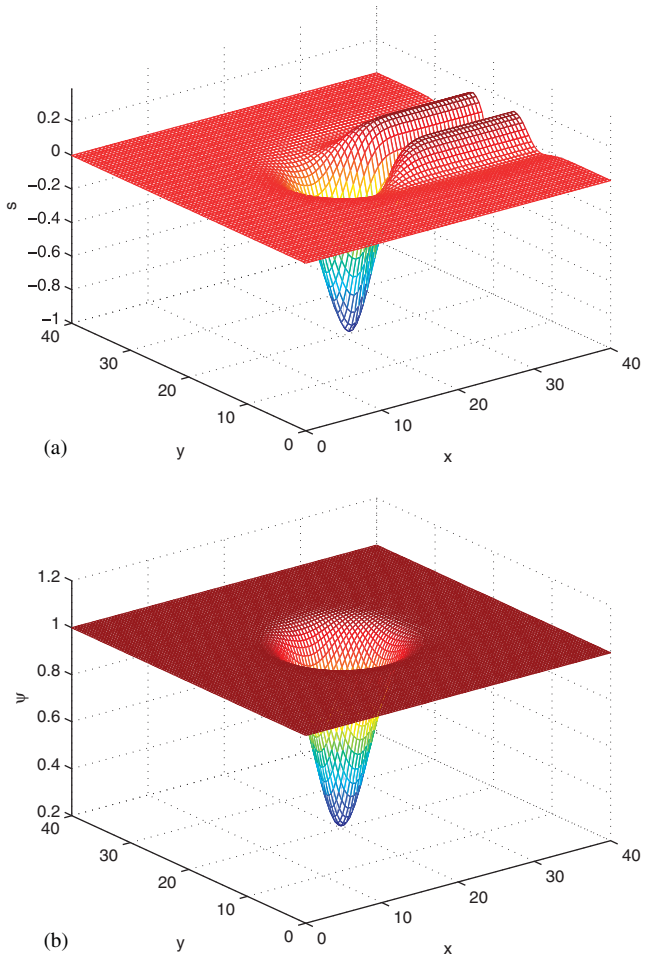

Figure 3. Bell-shaped free surface profile. The flow is in the positive x direction: (a) required substrate topography to obtain the free surface given by Equation (32) with $s_0 = -0.8$, $x_0 = y_0 = 20$, and $\delta = 4$ and (b) corresponding bell-shaped free surface profile.

them are obtained by using the following recurrence relations:

$$x^{i+1} = x^i - \left(\frac{\partial p^{ex}}{\partial x} - 2 \right)_{(x^i, y^i)} \Delta l \tag{29}$$

$$y^{i+1} = y^i - \left(\frac{\partial p^{ex}}{\partial y} \right)_{(x^i, y^i)} \Delta l \tag{30}$$

$$h^{i+1} = h^i \exp \left(\frac{\dfrac{\partial^2 p^{ex}}{\partial x^2} + \dfrac{\partial^2 p^{ex}}{\partial y^2}}{3} \Delta l \right) \tag{31}$$

DOI: 10.1002/fld

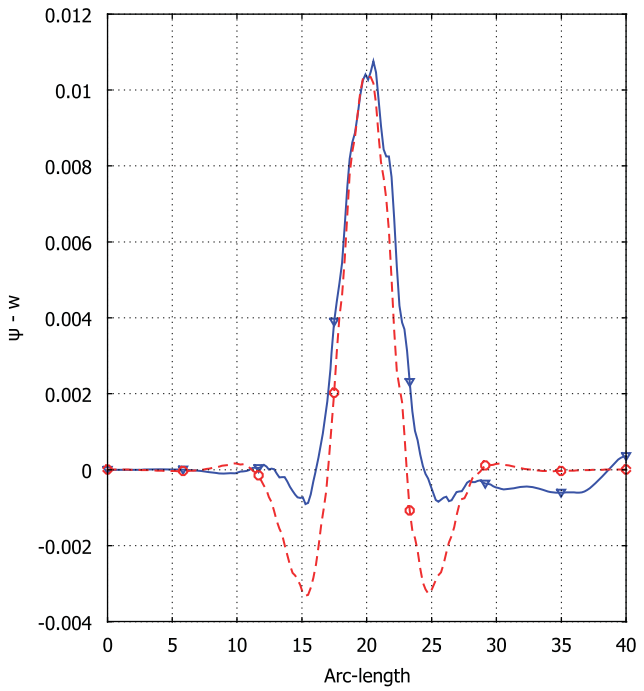

Figure 4. Difference between the computed and desired free surface profiles along the streamwise (solid line) and spanwise (dashed line) centerlines for the bell-shaped free surface profile.

subject to the initial conditions $h(x=0, y)=1$. The MATLAB program was used to implement the algorithm and post-process the results, [20].

4. RESULTS AND DISCUSSION

4.1. Validation cases without gravity

The first validation case consists in trying to give the free surface the bell profile given by

$$w(x, y)=1+s_0 e^{-\frac{(x-x_0)^2+(y-y_0)^2}{\delta^2}} \tag{32}$$

The obvious benefit of this profile being that it is infinitely differentiable so that the definition of the coefficients in Equation (17) is unambiguous and it satisfies $w(-\infty, y)=w(\infty, y)=1$. As discussed later, the inverse problem does not always admit a solution and the parameters, chosen for this test case and reported in the caption of Figure 3, were chosen such that a solution exists and the free surface displays a deep depression. The system of odes, Equations (18)–(20), is solved for 81 characteristics with the starting points uniformly distributed along $x=0$ and $\mathrm{d}l=0.01$. Having solved for h^i along the characteristics, the discrete topography values are easily recovered using the fact that $s^i=w^i-h^i$. The discrete topography values are then mapped onto a uniform (81×81) grid, which is imported into COMSOL to check whether the flow over the computed

DOI: 10.1002/fld

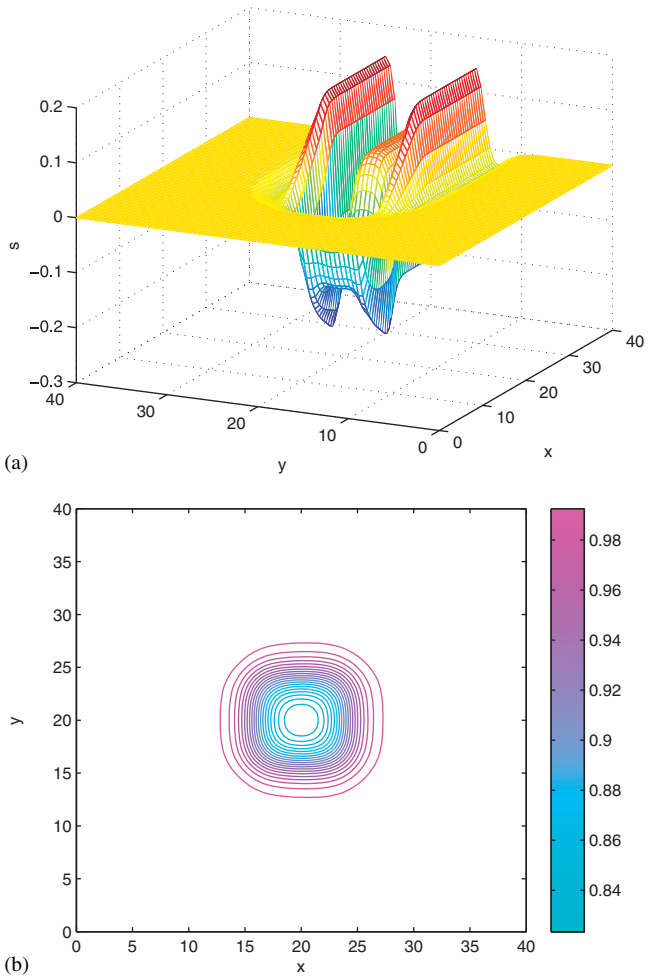

Figure 5. Square trench free surface profile: (a) required substrate topography to obtain the free surface given by $w(x, y) = 1 + s_{\tanh}(x, y)$ with $s_0 = -0.2$, $x_1 = 16$, $x_2 = 24$, $y_1 = 16$, $y_2 = 24$, and $\delta = 2$ and (b) corresponding square trench free surface contours. The flow is in the positive x direction.

topography profile results in the desired free surface profile. Figure 3(b) confirms that the proposed approach is successful since the free surface indeed appears to have the required bell profile. In fact, Figure 4, plotting the difference between the desired and computed free surface profiles along the streamwise and spanwise centerlines of the domain, reveals that the maximum difference is approximately 1.25% of the total free surface elevation range. As required, the downstream free surface disturbances have been annihilated by the substrate topography thereby, in a sense, beating capillarity. The substrate topography, shown in Figure 3(a), includes two ridges which extend with a constant profile indefinitely downstream. This is unfortunate from a practical perspective as it implies that in order to locally control the free surface to eliminate the free surface disturbances, the substrate has to be patterned indefinitely downstream. This feature is supported by the structure

DOI: 10.1002/fld

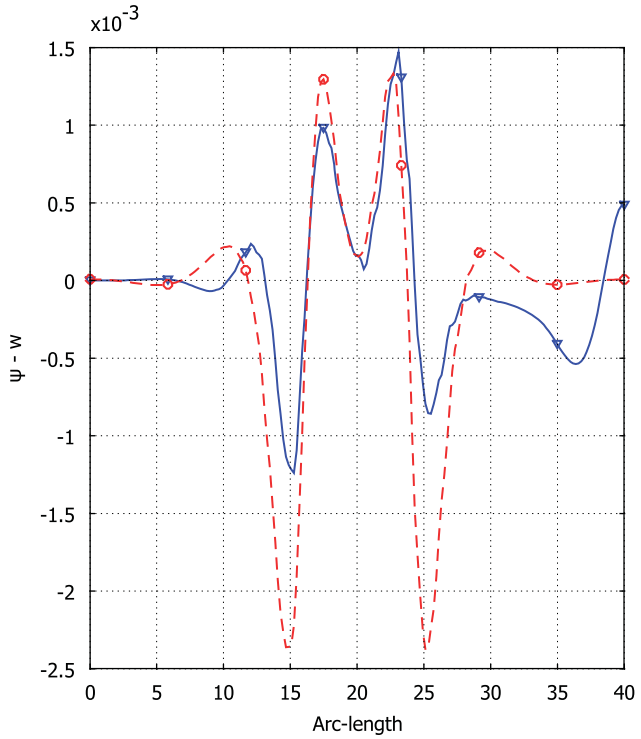

Figure 6. Difference between the computed and desired free surface profiles along the streamwise (solid line) and spanwise (dashed line) centerlines for the square trench free surface profile.

of the solution to the inverse problem described in the previous section. As the characteristic curves traverse the bell region where the cross-flow pressure gradient is non-zero, they are deflected according to Equation (19) and the film thickness satisfies Equation (28). As the characteristic curves leave the bell region and enter a region of zero pressure gradient, the film thickness must adopt a constant value according to Equation (26) with $\partial p^{ex}/\partial x = 0$. This constant value is set by matching the solution where a pressure gradient exists and where it does not. The set value of h is not necessarily equal to one and must remain unchanged downstream of the bell profile, which explains why the substrate topography must extend indefinitely downstream of the free surface defect.

The second validation case seeks the substrate design such that the free surface profile has the appearance of a square trench given by hyperbolic tangent functions according to $w(x, y) = 1 + s_{\tanh}(x, y)$ where $s_{\tanh}(x, y)$ is given by Equation (13). The 'walls' of the trench have hyperbolic tangent profiles and become steeper for smaller values of δ. The results, shown in Figures 5 and 6, confirm once more the validity of the approach. In fact, the maximum mismatch between the desired and computed free surface profiles, plotted in Figure 6, is on the order of 1% of the total free surface height variation. Again, it is quite remarkable that the complex substrate topography shown in Figure 5(a) produces the very symmetric square trench free surface profile of Figure 5(b).

DOI: 10.1002/fld

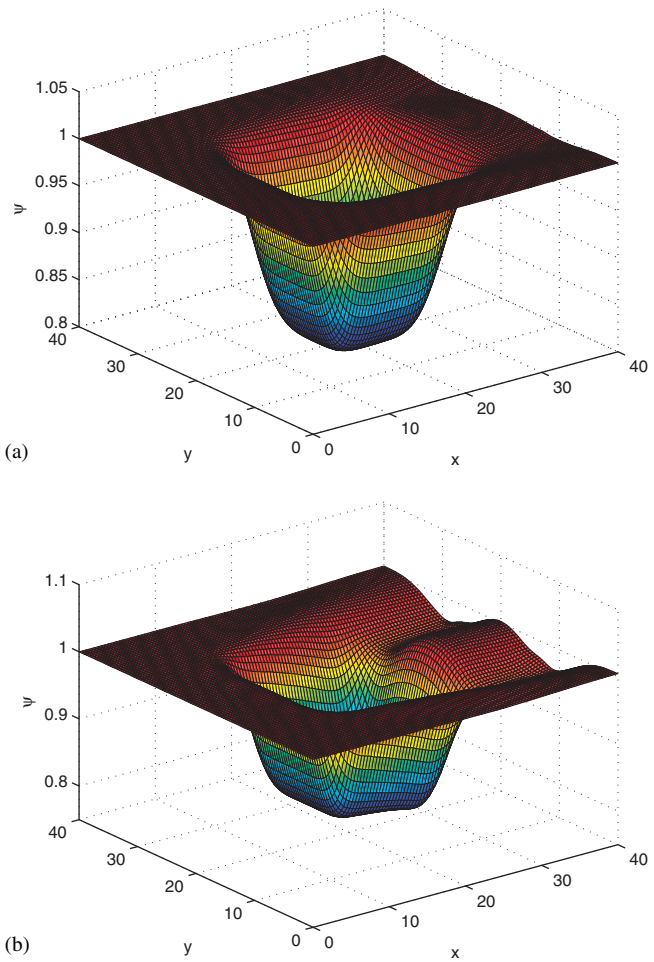

Figure 7. Computed free surface profile corresponding to the numerical solution to the inverse problem when $w(x, y) = 1 + s_{\tanh}(x, y)$ with $s_0 = -0.2$, $x_1 = 12$, $x_2 = 28$, $y_1 = 12$, $y_2 = 28$: (a) successful solution for $\delta = 2.1$ and (b) unsuccessful solution for $\delta = 1.5$.

4.2. Existence of a solution to the inverse problem

As one intuitively expects the free surface cannot sustain exceedingly sharp corners because of surface tension and the question arises as to how steep a step the free surface can take. To address this question, we use the same square trench free surface profile as above, vary the value of the steepness parameter δ, and assess the validity of the solution to the inverse problem by looking at the resulting free surface profile and computing the L_2 norm of the residuals according to

$$I = \frac{1}{2} \int_{\Omega} (\psi - w)^2 \, \mathrm{d}\omega \tag{33}$$

DOI: 10.1002/fld

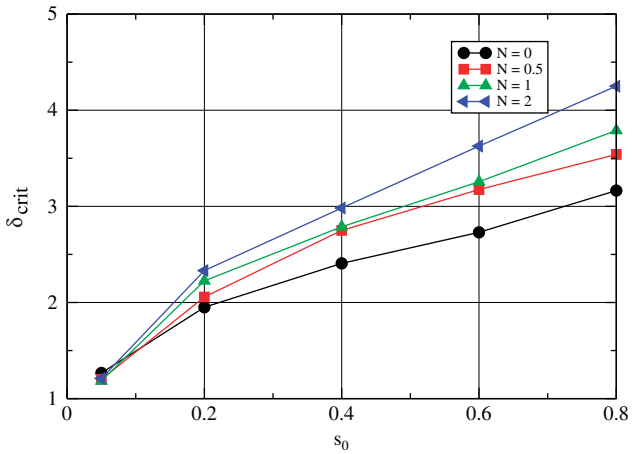

Figure 8. Threshold values of the steepness parameter δ_{crit} beyond, which a solution to the inverse problem exists for different values of the trench depth s_0 and the dimensionless parameter $N = Ca^{1/3}\cot(\alpha)$.

where the computational domain Ω extend to 40 L_d in either direction (or $\Omega = (40 \times 40)$ in dimensionless coordinates). The square trench extends over 16 L_d, a large enough value to decorrelate the effects of the step down (on the upstream side of the trench) and the step up (on the downstream side). Approximately 76% of the overall free surface height variation occurs in a 2δ interval surrounding the step. The free surface profile associated with a 'successful' solution to the inverse problem for $\delta = 2.1$ and an unsuccessful one for $\delta = 1.5$ are shown in Figures 7(a) and (b), respectively. Decreasing the value of δ makes the desired free surface profile steeper and more unlikely to be achieved. The naked eye clearly distinguishes the successful from the unsuccessful solutions as the free surface cannot recover its targeted value downstream of the topography for the unsuccessful case. This is more quantitatively reflected in the value of I, which is 4.96×10^{-3} in Figure 7(a) and 0.166 in Figure 7(b). In the following, a solution to the inverse problem will be deemed acceptable and therefore existing if $I \leqslant 10^{-2}$.

Figure 8 shows how the critical values of the steepness parameter δ_{crit}, beyond which a solution to the inverse problem exists, varies with the trench depth s_0 and the dimensionless parameter $N = Ca^{1/3}\cot(\alpha)$. Not surprisingly, the figure reveals that the deeper the trench profile, the larger the δ_{crit} value needs to be. In other words, larger free surface height variations need to occur over greater distances. This is a consequence of the fact that the free surface needs to keep its curvature as low as possible.

The effect of the normal component of gravity through the value of N is, on the other hand, more unexpected. The addition of a body force normal to the flow suggests that it should be easier to give the free surface a steeper profile. Figure 8, however, contradicts this intuition as δ_{crit} increases with N for a given value of s_0. This suggests that it is easier to control the free surface for lower values of N or equivalently lower values of the Capillary number Ca or larger values of α.

The previous results have established that the inverse problem only admits a solution for a limited range of the steepness parameter thereby confirming the insight that a free surface cannot sustain infinitely sharp corners. It was found, however, that steeper free surface profiles could be achieved by rotating the desired profile with respect to the direction of the flow. Figures 9(a)

DOI: 10.1002/fld

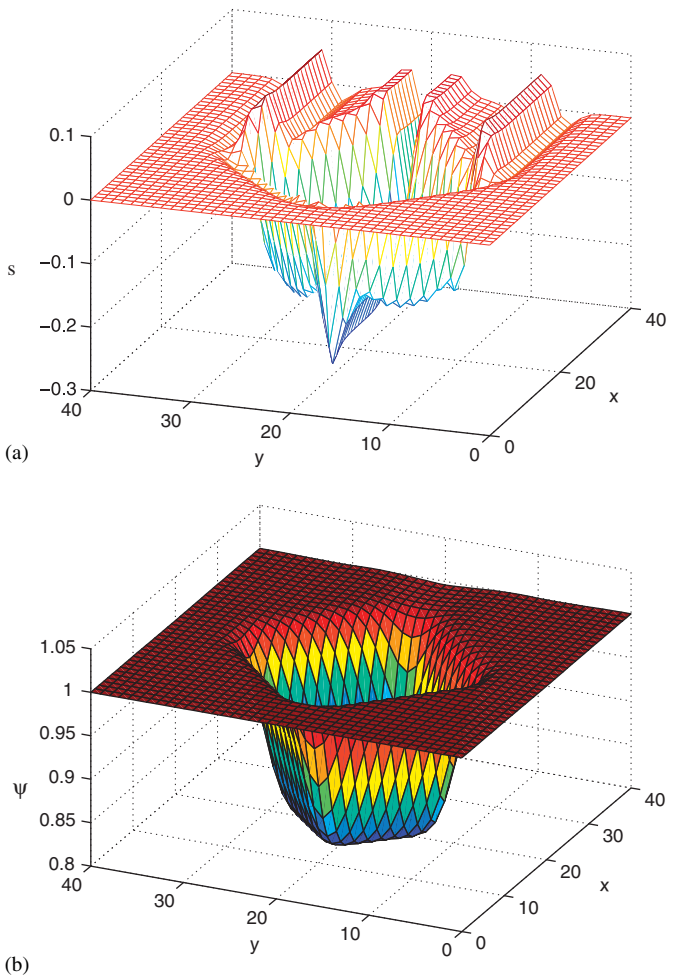

Figure 9. Diamond-shaped free surface profile. The flow is in the positive x direction: (a) required substrate topography to obtain the diamond-shaped free surface profile with $s_0 = -0.2$ and $\delta = 1.5$ and (b) corresponding free surface.

and (b), for example, show the required topography to obtain a trench free surface profile rotated by $\pi/4$ with respect to the direction of the flow , therefore having a diamond shape, with $N = 0$ and $s_0 = -0.2$. The critical value of δ is reduced from 2 when the desired profile is aligned with the flow to 1.4 when it is rotated.

4.3. Auxiliary application: substrate reconstruction

The method described in the previous section can be applied to another inverse problem of potential interest to thin layer flows. In this problem, the free surface elevation is known at a number of discrete points and the task is to reconstruct the substrate topography from this knowledge. This problem is non-trivial and an in-depth treatment of the question is beyond the scope of this paper

DOI: 10.1002/fld

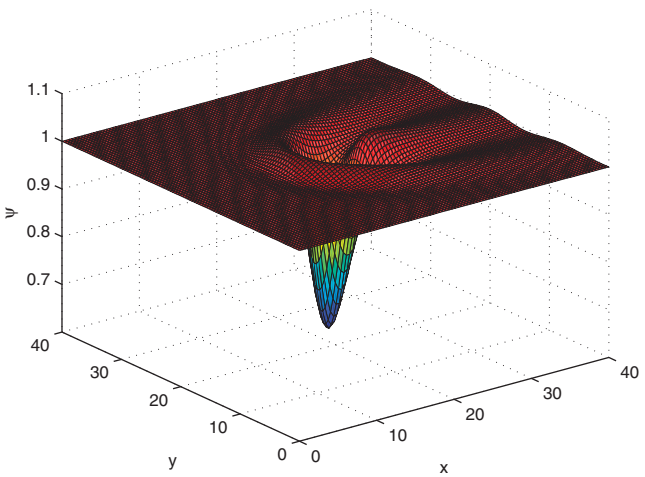

Figure 10. 'Experimental' free surface profile obtained using Equation (13) with $s_0 = -0.5, x_1 = 18, x_2 = 22, y_1 = 18, y_2 = 22$, and $\delta = 0.8$.

but a simple illustrative example is reported to confirm the validity of the abstract idea. Artificial 'experimental' data are obtained by performing a forward simulation with the substrate topography given by Equation (13) with $s_0 = -0.5$, $x_1 = 18$, $x_2 = 22$, $y_1 = 18$, $y_2 = 22$, and $\delta = 0.8$. The corresponding free surface profile can be seen in Figure 10. The free surface data are then mapped on a uniform (41×41) grid. In order to reconstruct the substrate profile, the pde (17) is solved using the method of characteristics as described above to evaluate the film thickness $h(x, y)$. Linear interpolation of the free surface elevation data is used to evaluate the coefficients of Equation (17), which directly depend on the derivatives of the free surface elevation. Clearly, for true experimental and noisy data, care would have to be taken for the evaluation of the derivatives. The substrate profile is then reconstructed by using the fact that $s(x, y) = \psi(x, y) - h(x, y)$. Figures 11(a) and (b) show the reconstructed and actual substrate profiles. While agreement between the two is not perfect, the depth and extent of topography are well captured by the reconstruction algorithm thereby confirming the validity of the idea in principle.

5. CONCLUSIONS

This paper demonstrates that in some cases and with a suitable substrate design, it is possible to give the free surface of a thin liquid film, a desired profile. This confirms that the effect of capillarity can be overcome and could have interesting implications for the micro-manufacturing of patterned functional layers for example. Remarkably, while the forward problem involves a fourth-order non-linear pde, the required substrate topography is inferred by solving a first-order linear pde, which is derived from the lubrication approximation. This results in an explicit formulation of the inverse problem in contrast with most inverse problems, which have to be solved by introducing an objective function and rely on the tools of optimization theory to find an optimal design. The main drawback of such techniques, which is the impossibility to guarantee that a global minimum has been identified is thus avoided. The first-order pde is solved numerically using the methods of

DOI: 10.1002/fld

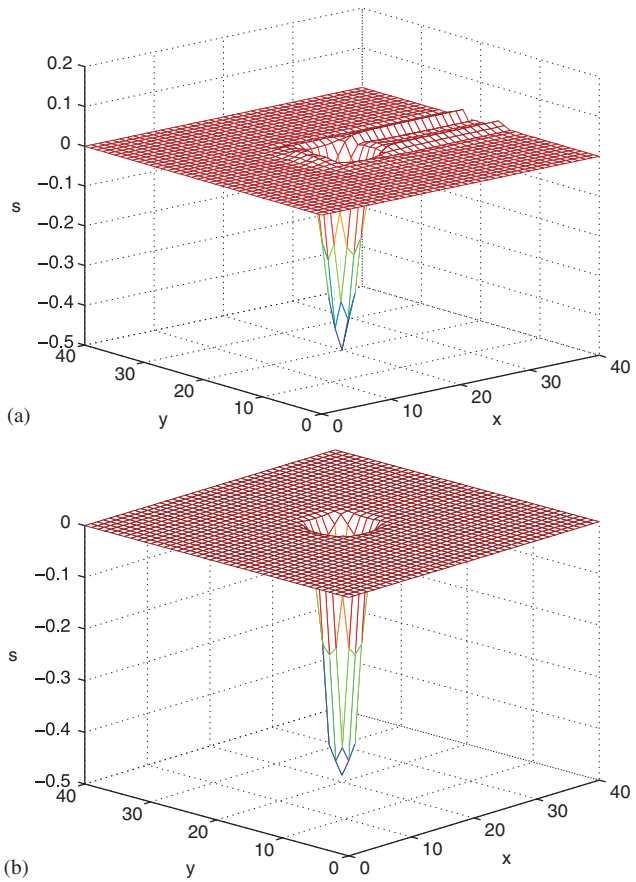

Figure 11. (a) Reconstructed substrate profile and (b) actual substrate profile.

characteristics. The resulting computed substrate designs have convoluted shapes and it is found that in order to control the free surface locally, the substrate pattern needs to extend indefinitely in the downstream direction. Expectedly, not every free surface profile can possibly be achieved and it is found that there exists a critical steepness of the free surface, which depends on the height of the free surface height variation and the normal component of gravity, beyond which a solution to the inverse problem does not exist. The proposed method has been applied to an interesting auxiliary problem, which involves substrate reconstruction from known free surface data. A similar technique could be used to solve other inverse problems related to thin layer flow such as bedrock reconstruction from free surface data in glacier flows for example.

REFERENCES

1. Decré MMJ, Baret JC. Gravity-driven flows of viscous liquids over two-dimensional topographies. *Journal of Fluid Mechanics* 2003; **487**:147–166.
2. Gramlich CM, Kalliadasis S, Homsy GM, Messer C. Optimal leveling of flow over one-dimensional topography by Marangoni stresses. *Physics of Fluids* 2002; **14**(6):1841–1850.

DOI: 10.1002/fld

3. Kalliadasis S, Bielarz C, Homsy GM. Steady free-surface thin film flows over topography. *Physics of Fluids* 2000; **12**(8):1889–1898.
4. Tseluiko D, Blyth MG, Papageorgiou DT, Vanden-Broeck JM. Electrified viscous thin film flow over topography. *Journal of Fluid Mechanics* 2008; **597**:449.
5. Gaskell PH, Jimack PK, Sellier M, Thompson HM, Wilson MCT. Gravity-driven flow of continuous thin liquid films on non-porous substrates with topography. *Journal of Fluid Mechanics* 2004; **509**:253–280.
6. Sellier M. Substrate design or reconstruction from free surface data for thin film flows. *Physics of Fluids* 2008; **20**:062106.
7. Jameson A. Aerodynamics design via control theory. *Journal of Scientific Computing* 1988; **3**:233–260.
8. Mohammadi B, Pironneau O. Shape optimization in fluid mechanics. *Annual Review of Fluid Mechanics* 2004; **36**:255–279.
9. Stillwagon LE, Larson RG. Leveling of thin films over uneven substrates during spin coating. *Physics of Fluids A* 1990; **2**(11):1937–1944.
10. Peurrung LM, Graves BG. Film thickness profiles over topography in spin coating. *Journal of the Electrochemical Society* 1991; **138**:2115–2124.
11. Hayes M, O'Brien SBG, Lammers JH. Green's function of a steady flow over a two-dimensional topography. *Physics of Fluids* 2000; **12**:1841–1858.
12. Kalliadasis S, Homsy GM. Stability of free-surface thin-film flows over topography. *Journal of Fluid Mechanics* 2001; **448**:387–410.
13. Davis JM, Troian SM. Generalised linear stability of noninertial coating flows over topographical features. *Physics of Fluids* 2005; **17**:072103.
14. Pozrikidis C, Thoroddsen ST. The deformation of a liquid film flowing down an inclined plane wall over a small particle arrested on the wall. *Physics of Fluids A* 1991; **11**:2546–2559.
15. Blyth MG, Pozrikidis C. Film flow down an inclined plane over a three-dimensional obstacle. *Physics of Fluids* 2006; **18**(5):052104.
16. Luo H, Pozrikidis C. Effect of inertia on film flow over oblique and 3-d corrugations. *Physics of Fluids* 2006; **18**:078107.
17. Luo H, Pozrikidis C. Gravity-driven film flow down an inclined wall with 3-d corrugations. *Acta Mechanica* 2007; **188**:209–225.
18. Lee YC, Thompson HM, Gaskell PH. An efficient adaptive Multigrid algorithm for predicting thin film flow on surfaces containing localised topographic features. *Computers and Fluids* 2007; **36**:838–855.
19. Sellier M, Lee YC, Thompson HM, Gaskell PH. Thin film flows on surfaces containing arbitrary occlusions. *Computer and Fluids* 2009; **38**:171–182.
20. The MathWorks, Inc. Matlab R2007b Documentation, 2007.

DOI: 10.1002/fld